Piezoelectricity of $SrTiO_3$: An *ab initio* description

A. Erba,[1,*] Kh. E. El-Kelany,[2,3] M. Ferrero,[1,2] I. Baraille,[2] and M. Rérat[2]

[1]*Dipartimento di Chimica and Centre of Excellence Nanostructured Interfaces and Surfaces (NIS), Università di Torino, via Giuria 5, IT-10125, Torino, Italy*

[2]*Equipe de Chimie Physique, IPREM UMR 5254, Université de Pau et des Pays de l'Adour, FR-64000, Pau, France*

[3]*Chemistry Department, Faculty of Science, Minia University, Minia 61519, Egypt*

(Received 2 April 2013; published 2 July 2013)

The complete piezoelectric tensor of ferroelectric $SrTiO_3$ at low temperature is computed by *ab initio* theoretical simulations. Both direct and converse—coupled with elastic compliance—piezoelectricity are computed and interpreted in terms of electronic and nuclear contributions. The role of the ferroelectric soft phonon mode on this property is found to be dramatic thus leading to a possible giant piezoelectric response at very low temperature. Two possible space groups are considered for the ferroelectric phase of $SrTiO_3$, both compatible with the available experimental data: a tetragonal $I4cm$ and an orthorhombic $Ima2$ one. The piezoelectric response of the two symmetries is predicted to be rather different and could be experimentally detected to clarify the (still unknown) structure of the ferroelectric phase of $SrTiO_3$.

DOI: 10.1103/PhysRevB.88.035102 PACS number(s): 31.15.A−, 77.84.−s

I. INTRODUCTION

Standard piezoelectric ceramics, such as lead zirconate titanate (PZT) based materials, are widely used as sensor and actuator devices, hydrophones, multilayered capacitors, ultrasonic motors, transformers, and medical ultrasonics devices for acoustic radiation force impulse imaging.[1,2] Such materials could be used for several applications at cryogenic temperatures such as actuators for adaptive optics (space telescopes and low-temperature capacitors, for instance); however, their piezoelectric response is significantly reduced at very low temperatures. In 1997, Grupp and Goldman discovered a giant piezoelectric effect of strontium titanate ($SrTiO_3$) down to 1.6 K, where the sole *converse* piezoelectric coefficient $d_{31} = 16 \times 10^{-10}$ m/V was reported which is comparable to those of PZT at room temperature. These findings opened the way for applications of $SrTiO_3$ in ultralow-temperature scanning microscopies and magnetic field-insensitive thermometers.[3] Till now, this remained the only experimental determination of a piezoelectric constant of $SrTiO_3$, whose complete *direct* and *converse* third-order piezoelectric tensors still have to be determined and discussed. Even theoretically, only a few features of the *direct* piezoelectric tensor **e** have been reported: Furuta and Miura[4] computed two constants, e_{31} and e_{33}, with an in-plane compressive tetragonal structure while Naumov and Fu[5] computed the quantity $e_{33} - e_{31}$—which corresponds to the piezoelectric response to a tetragonal strain at fixed volume—of cubic $SrTiO_3$ under a finite electric field. In what follows we shall briefly recall the main structural and electronic features of $SrTiO_3$.

$SrTiO_3$ is probably the most studied complex oxide perovskite of the ABO_3 family due to its many technological applications in optoelectronics, macroelectronics, and ferroelectricity (see Ref. 6 and references therein). This material exhibits an impressive variety of peculiar properties: a colossal magnetoresistance,[7] anomalously large dynamical effective charges resulting in a giant longitudinal optical-transverse optical (LO-TO) splitting,[8] the huge zero-point motion of Ti ions,[9] giant elastic softening (superelasticity) at low temperature,[10] extremely large dielectric constants which increase when the temperature decreases,[11,12] superlattice high-T_c superconductivity,[13] anomalous ferroelasticity,[14] and so on.

At room temperature, $SrTiO_3$ crystallizes in a simple cubic structure of space group $Pm\bar{3}m$ where each Ti ion is octahedrally coordinated to six O ions. This arrangement of atoms shows at least two types of structural instabilities, each connected to a particular soft phonon mode of its first Brillouin zone (BZ): a structural R-point rotation of TiO_6 octahedra and a Γ-point ferroelectric displacement of Ti ions from the center of the octahedra. On cooling, $SrTiO_3$ undergoes a second-order antiferrodistortive (AFD) phase transition at $T_a = 105$ K to a tetragonal phase with space group $I4/mcm$. The tetragonal phase is characterized by static rotations of TiO_6 octahedra around the tetragonal axis c and by a slight unit-cell stretching; the crystallographic axes of the AFD phase are rotated by 45° around the c axis of the cubic phase. Two order parameters are associated with this phase transition: the octahedra-rotation angle θ (reported to be 2.1° at 4.2 K) (Ref. 15) and the tetragonality of the unit cell c/a (reported to be 1.0009 at 10 K) (Ref. 16). In recent years, many theoretical investigations have helped in clarifying the specific aspects of this transition,[6,17–22] which was recently found to be fully describable by classical Landau theory with terms up to the sixth order of the free energy expansion.[23]

By further cooling below T_a, down to about 50 K, the ferroelectric instability leads to a softening of the Ti-displacement phonon mode and to anomalously large values of the static dielectric constants which grow according to a Curie-Weiss law. A ferroelectric phase transition could be expected to occur at $T_f \sim 35$ K; however, below a certain temperature $T_q = 37$ K, these quantities saturate and the ferroelectric transition is suppressed down to 0 K by strong zero-point quantum fluctuations.[12,24] $SrTiO_3$ then remains in a quantum coherent state (also called the Müller state after its discoverer) even at very low temperatures where it becomes a so-called *quantum paraelectric*.[25]

It has been known for a long time that a ferroelectric transition to a lower (unknown) symmetry phase can be

induced by applying to $SrTiO_3$ either an electric field[26] along c or a stress perpendicularly to c (Refs. 27,28). It has even been reported that room-temperature ferroelectricity can be achieved by epitaxial strain.[29] More recently, it has been found that the transition can also be driven by doping with Ca or Bi atoms[30,31] and by isotope substitution: when ^{16}O atoms are fully replaced by their ^{18}O isotopes, a ferroelectric transition occurs at $T_f = 24$ K (Refs. 32,33). Many optical and spectroscopic measurements have been performed on this ferroelectric phase $SrTi^{18}O_3$: Raman,[34,35] hyper-Raman,[36] Brillouin scattering,[37] and birefringence.[38] All these analyses reported qualitative evidence of the ferroelectric transition, confirming a reduction of the symmetry. Evidence of structural changes are rare: only a recent neutron scattering experiment has revealed a lowering of the symmetry to a phase that is most likely to be orthorhombic.[39] The orthorhombic symmetry of the ferroelectric phase of $SrTi^{18}O_3$ has also been supported by *ab initio* theoretical phonon calculations that suggest the $Ima2$ space group.[40]

In this work, we report accurate *ab initio* simulations of the complete *direct* and *converse* third-rank piezoelectric tensors **e** and **d** of ferroelectric $SrTiO_3$, as well as of its elastic $\mathbb{C}$ and compliance $\mathbb{S}$ fourth-rank tensors. Electronic and nuclear relaxation (dynamical) contributions to the piezoelectricity are presented. Effective Born charges, phonon frequencies, and the effect of nuclear vibrations on the dielectric tensor ϵ are also discussed in connection to the piezoelectric properties of $SrTiO_3$. Two different possible symmetries are considered for the ferroelectric low-temperature phase of $SrTiO_3$, a tetragonal $I4cm$ and an orthorhombic $Ima2$; the effect of the different symmetries on the computed piezoelectric response is analyzed.

The calculations are performed using a basis set of atom-centered Gaussian-type functions (GTF). Five different one-electron Hamiltonians are considered: the reference Hartree-Fock (HF) method, a local density approximation (LDA), and a generalized gradient approximation (GGA), namely Perdew-Burke-Ernzerhof (PBE),[41] to the density functional theory (DFT), and a hybrid scheme (namely PBE0)[42] which includes 25% of the exact HF exchange. The CRYSTAL program for solid state quantum chemistry is used.[43,44]

The structure of the paper is as follows. In Sec. II we briefly illustrate the theoretical methods used for the calculation of phonon frequencies, dielectric constants, effective Born charges, and elastic and piezoelectric constants and we report the main computational parameters adopted for the calculations, whose effect is discussed in Sec. III A where the definition of an optimal setup is sought after. The subsequent sections present the main results on the structural, vibrational, and piezoelectric properties of $SrTiO_3$. Conclusions and perspectives are drawn in Sec. IV.

II. COMPUTATIONAL METHOD AND DETAILS

All the calculations reported in the paper are performed with the program CRYSTAL for *ab initio* quantum chemistry of a solid state.[43,44] An atom-centered Gaussian-type-orbital basis set is adopted which has been obtained by adding further polarization functions to the one used by Evarestov *et al.*[20] and is available on the web:[45] an all-electron split-valence 8-411G($2d1f$) for the O atoms, an all-electron split-valence 86-411($2d1f$) for Ti atoms while the core of Sr atoms is described by a Hay-Wadt effective-core pseudopotential[46] and the valence by 211G($2d1f$) functions.

In CRYSTAL, the truncation of infinite lattice sums is controlled by five thresholds, which are here set to 10, 10, 10, 12, and 24 and whose effect is commented on in Sec. III A. Reciprocal space is sampled according to a sublattice with a shrinking factor of 8. The DFT exchange-correlation contribution is evaluated by numerical integration over the cell volume: radial and angular points of the atomic grid are generated through Gauss-Legendre and Lebedev quadrature schemes using an accurate predefined pruned grid. The accuracy in the integration procedure can be estimated by evaluating the error associated with the integrated electronic charge density in the unit cell versus the total number of electrons per cell: $1 \times 10^{-5}|e|$ out of a total number of 112 electrons per cell for the orthorhombic phase, for instance. For any further detail about the grid generation and its influence on the accuracy and cost of the calculations, see Refs. 47–49 and the discussion of Sec. III A. The convergence threshold on energy for the self-consistent-field (SCF) step of the calculations is set to 10^{-10} hartree for geometry optimizations and to 10^{-11} hartree for phonon frequency calculations.

All structures have been optimized by the use of analytical energy gradients with respect to both atomic coordinates and unit-cell parameters,[50–52] with a quasi-Newtonian technique combined with the Broyden-Fletcher-Goldfarb-Shanno (BFGS) algorithm for Hessian updating.[53–56] Convergence has been checked on both gradient components and nuclear displacements; the corresponding tolerances on their root mean square are set to 0.0003 and 0.0012 a.u., respectively.

The calculation of vibration frequencies has been performed within the harmonic approximation to the lattice potential. Details on the calculation of vibrational frequencies with CRYSTAL can be found elsewhere[57,58] as well as some recent examples of the application.[59,60] Here, let us simply remind that vibration frequencies at the Γ point of the BZ can be obtained from the diagonalization of the mass-weighted Hessian matrix of the second derivatives of the total energy per cell with respect to pairs of atomic displacements in the reference cell. The first derivatives are computed analytically, whereas the second derivatives are computed numerically.

A. Dielectric tensor

The electronic contribution to the static dielectric tensor is evaluated through a coupled-perturbed Hartree-Fock/Kohn-Sham scheme[61] adapted to periodic systems.[62] This is a perturbative, self-consistent method that focuses on the description of the relaxation of the crystalline orbitals under the effect of an external electric field. The perturbed wave function is then used to calculate the dielectric properties as energy derivatives. Further details about the method and its implementation in the CRYSTAL program can be found elsewhere[63–65] as well as some recent examples of its application.[59,66–68] The total static dielectric tensor is the sum of the electronic and the vibrational

contributions

$$\epsilon_{ij}^{0} = \epsilon_{ij}^{\rm el} + \epsilon_{ij}^{\rm vib} = \epsilon_{ij}^{\rm el} + \frac{4\pi}{V}\sum_{p}\frac{Z_{p,i}Z_{p,j}}{\nu_p^2}\,, \qquad (1)$$

where ν_p is the phonon frequency of mode p, V is the unit cell volume, and $\mathbf{Z}_p$ is the mass-weighted mode effective Born vector.[69] Atomic Born effective tensors and mode effective Born vectors can be computed with the CRYSTAL program through a Berry-phase approach.[70,71] The intensity $\mathcal{I}_p$ of IR absorbance for a given mode p is proportional to $|\mathbf{Z}_p|^2$.

B. Piezoelectric tensors calculation

In the linear regime, *direct* **e** and *converse* **d** piezoelectric tensors describe the polarization **P** induced by strain η and the strain induced by an external electric field **E**, respectively,

$$\textit{direct}\ \text{effect} \quad \mathbf{P} = \mathbf{e}\,\eta \quad \text{at constant field}, \qquad (2)$$

$$\textit{converse}\ \text{effect} \quad \eta = \mathbf{d}^T\mathbf{E} \quad \text{at constant stress}. \qquad (3)$$

Our approach consists in directly computing the intensity of the polarization induced by strain. The Cartesian components of the polarization can then be expressed as follows in terms of the strain tensor components:

$$P_i = \sum_v e_{iv}\eta_v \quad \text{so that} \quad e_{iv} = \left(\frac{\partial P_i}{\partial \eta_v}\right)_E . \qquad (4)$$

In the above expression, $i = x,y,z$; η is the pure strain tensor, the derivative is taken at constant electric field, and Voigt's notation is used according to which $v = 1,\ldots,6$ ($1 = xx$, $2 = yy$, $3 = zz$, $4 = yz$, $5 = xz$, $6 = xy$) (Ref. 72). In CRYSTAL the polarization can be computed either via localized Wannier functions or via the Berry phase (BP) approach.[73] The latter scheme is used in the present work according to which direct piezoelectric constants can be written as follows in terms of the numerical first derivatives of the BP φ_l with respect to the strain:[70,74,75]

$$e_{iv} = \frac{|e|}{2\pi V}\sum_l a_{li}\frac{\partial \varphi_l}{\partial \eta_v}\,, \qquad (5)$$

where a_{li} is the ith Cartesian component of the lth direct lattice basis vector $\mathbf{a}_l$. The derivatives in the right-hand side of Eq. (5) are computed numerically by applying finite strains to the crystal lattice.

A simple connection exists between the *direct* and *converse* piezoelectric tensors

$$\mathbf{e} = \mathbf{d}\,\mathbb{C} \quad \text{and} \quad \mathbf{d} = \mathbf{e}\,\mathbb{S}\,, \qquad (6)$$

where $\mathbb{C}$ is the fourth-rank elastic tensor of energy second derivatives with respect to pairs of deformations and $\mathbb{S} = \mathbb{C}^{-1}$ is the fourth-rank compliance tensor. For any detail about the numerical accuracy of elastic and piezoelectric calculations with the CRYSTAL program we refer to previous works.[76]

We recall that piezoelectric constants can be decomposed into purely electronic "clamped-ion" and nuclear "internal-strain" contributions, as for the dielectric tensor, $e_{iv} = e_{iv}^{\rm clamp} + e_{iv}^{\rm relax}$; the nuclear term measures the piezoelectric effect due to relaxation of the relative positions of atoms induced by the strain[77,78] and can be computed by optimizing the atomic positions within the strained cell.

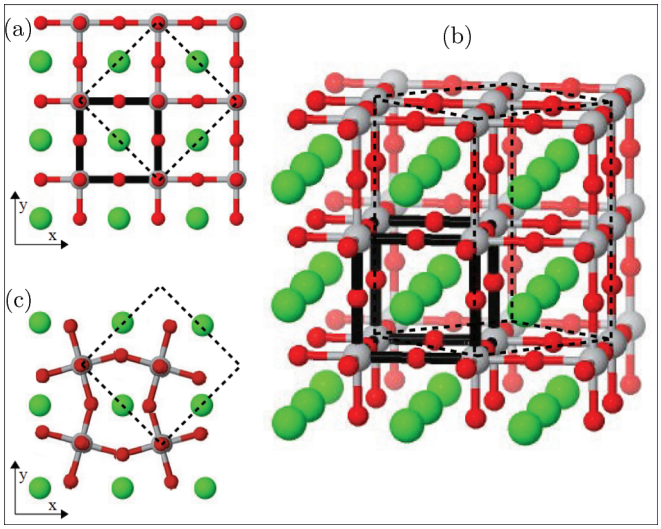

FIG. 1. (Color online) Graphical representation of the structure of $SrTiO_3$. In panel (a), the cubic $Pm\bar{3}m$ phase is represented in the xy plane; the conventional cubic cell (thick continuous line) and the quadruple pseudocubic tetragonal cell (dashed line) are shown which contain 5 and 20 atoms, respectively. The same structure and cells are also represented in a different view in panel (b). Panel (c) reports the structure of the $I4/mcm$ tetragonal phase in the xy plane; rotation of adjacent TiO_6 octahedra (largely magnified for making it visible) can be inferred from comparison with panel (a). These pictures have been prepared using the J-ICE online interface to Jmol (Ref. 79).

III. RESULTS AND DISCUSSION

Before presenting our results, let us briefly describe which are the structural features of the four models we use for $SrTiO_3$. At room temperature, $SrTiO_3$ exhibits a simple cubic $Pm\bar{3}m$ structure (see Fig. 1) whose crystallographic cell contains five atoms and is characterized by three identical lattice parameters $a = b = c = a_0$. Ti atoms are found at the vertices of the cube, O atoms at the midpoints of cube edges, and a Sr atom occupies the cube center. Let us introduce a quadruple pseudocubic cell, which will prove useful in the subsequent discussion, by doubling the lattice parameter along z ($c = 2a_0$) and by doubling the cell in the xy plane so that $a = b = \sqrt{2}a_0$. Such a pseudocubic cell is represented in Fig. 1 in the dashed lines.

Below $T_a = 105$ K, $SrTiO_3$ undergoes a transition to a tetragonal phase of $I4/mcm$ symmetry, whose crystallographic cell contains 20 atoms and almost coincides with the pseudocubic cell, apart from a rotation of the adjacent TiO_6 octahedra along the z direction of an angle θ [as can be inferred by comparing Figs. 1(a) and 1(c)] and a slight deviation from the pseudocubic ratio $c/2a_0 = 1$. A structural parameter u (0.25 in the pseudocubic structure) is considered, which corresponds to the fractional coordinate along z of the O atom in the 8*h* Wyckoff position; its value is related to the octahedra rotation angle θ according to the relation $\theta = \arctan(1 - 4u)$.

Starting from the $I4/mcm$ tetragonal phase, the symmetry has been lowered to describe a ferroelectric phase to both a

tetragonal $I4cm$ and a orthorhombic $Ima2$ one. In both cases, a further structural parameter appears, $|\delta|$, which measures the displacement of Ti atoms from their equilibrium positions in the $Pm\bar{3}m$ and $I4/mcm$ phases. Note that, while in the tetragonal $I4cm$ structure Ti atoms are symmetry-constrained to move along the z direction, in the orthorhombic $Ima2$ structure they can move in the xy plane, much more along the x direction than along the y direction.

A. Definition of an optimal computational setup

The structural changes among the different phases of $SrTiO_3$ are quite small, though their effects on several properties turn out to be paramount, as discussed in the Introduction. The accuracy of *ab initio* simulations in reproducing basic structural and electronic properties has to be carefully checked before computing more sophisticated quantities. In particular, in this section, we discuss the effect of the adopted Hamiltonian and of two computational parameters: the DFT integration grid and the bi-electronic integrals tolerances. The radial and angular points of the atomic grid are generated through Gauss-Legendre and Lebedev quadrature schemes; each grid is labeled with the symbol (n_r,n_a) where n_r represents the number of radial points and n_a the maximum number of angular points. The truncation of infinite lattice sums for the integrals evaluation is controlled by five thresholds in the CRYSTAL program.[43]

A number of structural and electronic parameters of the four phases (namely, pseudocubic $Pm\bar{3}m$, $I4/mcm$, $I4cm$, and $Ima2$) considered are reported in Table I. Along with the structural parameters, already defined at the beginning of Sec. III, the direct band gap E_g and the difference between the cubic phase energy and that of the other phases ΔE^c are reported as well. All the values reported have been obtained by fully optimizing the structures at the PBE0 level.

Let us first consider the effect of the DFT grid; grid $G_1 = (55,434)$, which usually performs rather well, is found to describe very poorly even the two simple structures of cubic and tetragonal AFD phases. The structural and electronic parameters provided by grid $G_2 = (75,974)$ are already quite converged, if compared to those obtained with a richer grid $G_3 = (99,1454)$. This is especially so for the first two structures in the table. The only two (coupled) parameters that still vary when passing from G_2 to G_3 are u and angle θ for the two ferroelectric structures $I4cm$ and $Ima2$ thus revealing a particularly flat potential energy surface in that region. However, the most relevant structural parameter to piezoelectricity, that is, the displacement $|\delta|$ of Ti atoms, is already converged with G_2 in both structures. The G_2 grid will be used in the following.

In general, all the structural parameters are found to be more stable with respect to the integrals' tolerances. A $T_2 = (10,10,10,12,24)$ set slightly improves upon $T_1 = (8,8,8,8,16)$ and is almost at convergence if compared to a richer set $T_3 = (12,12,12,15,30)$. Again, this is particularly so for the two simplest structures. In the following, we will use the T_2 set of integral tolerances.

Finally, by recalling that calculations refer to 0 K, let us note that, regardless of the specific setting, the tetragonal AFD $I4/mcm$ phase is always electronically more stable than the cubic $Pm\bar{3}m$ one. The two ferroelectric phases are always electronically more stable than the AFD one, with the orthorhombic $Ima2$ in turn more stable than the tetragonal $I4cm$.

TABLE I. Influence of the DFT integration grid and electronic integral tolerances on computed structural and electronic properties (as defined in the text) of the four structures of $SrTiO_3$ here considered. Three DFT grids (n_r,n_a) with n_r radial points and a maximum of n_a angular points are used: $G_1 = (55,434)$, $G_2 = (75,974)$, and $G_3 = (99,1454)$. Three sets of integral tolerances are considered: $T_1 = (8,8,8,8,16)$, $T_2 = (10,10,10,12,24)$, and $T_3 = (12,12,12,15,30)$. Calculations are performed with the PBE0 hybrid functional.

	DFT Grid			Integral Tolerances		
	G_1	G_2	G_3	T_1	T_2	T_3
$Pm\bar{3}m$						
$a = b$ (Å)	5.480	5.505	5.505	5.505	5.505	5.505
c (Å)	7.750	7.785	7.785	7.786	7.785	7.785
E_g (eV)	4.141	4.110	4.110	4.088	4.110	4.126
$I4/mcm$						
$a = b$ (Å)	5.481	5.501	5.501	5.502	5.501	5.501
c (Å)	7.816	7.792	7.792	7.793	7.792	7.792
u	0.226	0.239	0.239	0.238	0.239	0.239
θ (deg)	5.484	2.519	2.519	2.748	2.519	2.519
E_g (eV)	4.225	4.135	4.135	4.177	4.135	4.149
ΔE^c (mHa)	2.207	0.029	0.015	0.023	0.029	0.035
$I4cm$						
$a = b$ (Å)	5.481	5.500	5.502	5.499	5.500	5.500
c (Å)	7.816	7.798	7.796	7.808	7.798	7.798
u	0.226	0.240	0.242	0.238	0.240	0.240
θ (deg)	5.484	2.291	1.833	2.748	2.291	2.291
$\|\delta\|$ (Å)	0.012	0.037	0.041	0.047	0.037	0.037
E_g (eV)	4.225	4.154	4.150	4.155	4.154	4.169
ΔE^c (mHa)	2.208	0.031	0.019	0.037	0.031	0.040
$Ima2$						
a (Å)	5.481	5.504	5.506	5.504	5.504	5.502
b (Å)	5.482	5.503	5.504	5.504	5.503	5.503
c (Å)	7.816	7.789	7.787	7.792	7.789	7.791
u	0.226	0.239	0.241	0.241	0.239	0.239
θ (deg)	5.484	2.519	2.062	2.063	2.519	2.519
$\|\delta\|$ (Å)	0.008	0.016	0.018	0.017	0.016	0.015
E_g (eV)	4.224	4.153	4.152	4.129	4.153	4.167
ΔE^c (mHa)	2.208	0.041	0.031	0.043	0.041	0.042

1. Effect of the Hamiltonian

In this section we briefly discuss the effect of the adopted one-electron Hamiltonian on the structural properties of the four $SrTiO_3$ phases. The structural properties, as obtained with the four Hamiltonians considered, are reported in Table II. To validate the accuracy of the present calculations, we compare both with the experiments and the theoretical results by El-Mellouhi *et al.*,[21] obtained with the screened hybrid Heyd-Scuseria-Ernzerhof 06 (HSE06) functional,[80] which have been recently reported and declared to constitute one of the most accurate *ab initio* datasets in the literature as concerns $SrTiO_3$.

From the analysis of cubic $Pm\bar{3}m$ and tetragonal $I4/mcm$ structures, for which accurate experimental data are available,

TABLE II. Influence of the adopted one-electron Hamiltonian on computed structural and electronic properties (as defined in the text) of the four structures of $SrTiO_3$ here considered. The pseudocubic structure is considered for comparison with the others.

	Present Study				Ref. 21	
	HF	LDA	PBE	PBE0	HSE06	Exp.
$Pm\bar{3}m$						
$a = b$ (Å)	5.529	5.453	5.563	5.505	5.518	5.501 (Ref. 81)
c (Å)	7.819	7.711	7.867	7.785	7.804	7.780 (Ref. 81)
E_g (eV)	12.203	1.906	1.901	4.110	3.590	3.75 (Ref. 82)
$I4/mcm$						
$a = b$ (Å)	5.528	5.441	5.554	5.501	5.515	5.507 (Ref. 9)
c (Å)	7.816	7.730	7.881	7.792	7.809	7.796 (Ref. 9)
$c/2a_0$	1.000	1.005	1.003	1.001	1.001	1.001 (Ref. 9)
u	0.249	0.228	0.231	0.239	0.241	0.240 (Ref. 15)
θ (deg)	0.229	5.029	4.346	2.519	2.010	2.1 (Ref. 15)
E_g (eV)	12.204	2.014	1.974	4.135	3.227	3.246 (Ref. 83)
ΔE^c (mHa)	−0.001	0.246	0.155	0.029	0.013	
$I4cm$						
$a = b$ (Å)	5.529	5.442	5.551	5.500		
c (Å)	7.818	7.729	7.900	7.798		
$c/2a_0$	1.000	1.002	1.004	1.002		
u	0.249	0.229	0.231	0.239		
θ (deg)	0.229	4.802	4.346	2.519		
$\lvert\delta\rvert$ (Å)	0.013	0.008	0.053	0.037		
E_g (eV)	12.203	2.010	2.014	4.154		
ΔE^c (mHa)	0.000	0.243	0.169	0.031		
$Ima2$						
a (Å)	5.527	5.440	5.559	5.504		
b (Å)	5.529	5.442	5.558	5.503		
c (Å)	7.819	7.729	7.879	7.789		
$c/2a_0$	1.000	1.002	1.002	1.001		
u	0.249	0.228	0.230	0.239		
θ (deg)	0.229	5.029	4.574	2.519		
$\lvert\delta\rvert$ (Å)	0.009	0.007	0.031	0.016		
E_g (eV)	12.205	2.013	2.018	4.153		
ΔE^c (mHa)	0.062	0.248	0.176	0.041		

it can be noticed that the pure generalized-gradient PBE functional overestimates the lattice parameters by 1.1% and HF by 0.5%, while a simple LDA functional underestimates them by 1.2%. The global hybrid PBE0 functional provides excellent lattice parameters for both structures with an overall error of 0.06%.

The HF description of the AFD phase is quite poor: along with the usual huge electronic band gap of 12.2 eV, with respect to an experimental value of 3.2 eV, it describes a very small distortion with respect to the pseudocubic structure. The rotation angle θ of the octahedra is very small, 0.2° with an experimental value of 2.1° at 4 K, the stretching of the cell is null ($c/2a_0 = 1.000$), and the electronic relative stability of the AFD phase with respect to the cubic is inverted. LDA overestimates the rotation angle θ, more so than PBE and PBE0, which provides a reasonable agreement with the experiment.

For each Hamiltonian, given the description of the first two structures, we expect a similar description also for the two ferroelectric phases for which structural experimental data are not presently available. The hybrid PBE0 functional guarantees a good description of the structural and electronic properties of $SrTiO_3$ and it constitutes our choice for the next calculations of phonon frequencies in Sec. III B and the elastic and piezoelectric constants in Sec. III C. The PBE0 results of the present work provide as good an agreement with the experiments as that obtained by El-Mellouhi *et al.*[21] in their study with a screened hybrid HSE06 (as can be inferred form the comparison of the two corresponding columns in Table II).

B. Phonon frequencies

We have anticipated in the Introduction that, due to an anomalously large zero-point motion,[9] the many peculiar properties of $SrTiO_3$, such as giant LO-TO splitting, giant elastic softening, and colossal magnetoresistance, strongly depend on their soft phonon modes. In particular, its giant piezoelectricity at low temperature is due to Ti atoms' displacements from their equilibrium positions. The aim of this section is to discuss the vibration phonon frequencies of $SrTiO_3$ and particularly their evolution when passing from the pseudocubic structure to AFD $I4/mcm$ and ferroelectric

TABLE III. Phonon wave numbers $\bar{\nu}$ (cm^{-1}), infrared intensity $\mathcal{I}_p$ (km/mol), and vibrational contribution to the dielectric tensor ϵ^{vib} (for the first three structures, parallel and perpendicular components refer to the z direction) for each mode p of the four $SrTiO_3$ structures considered. Dashes indicate null values. IR intensities and vibrational contributions to the dielectric tensors are not reported for imaginary phonon frequencies (crosses). The last two rows report the total vibrational and electronic contributions to ϵ. Values obtained with the PBE0 hybrid functional. Experimental values are from Refs. 34,84–86. The symmetry labeling of the modes according to the irreps of the various structures can be found in Refs. 20,34,40.

Cubic $Pm\bar{3}m$					Tetragonal $I4/mcm$					Tetragonal $I4cm$					Orthorhombic $Ima2$					
$\bar{\nu}_{calc}$	$\bar{\nu}_{exp}$	$\mathcal{I}_p$	$\epsilon^{vib}_{\parallel}$	$\epsilon^{vib}_{\perp}$	$\bar{\nu}_{calc}$	$\bar{\nu}_{exp}$	$\mathcal{I}_p$	$\epsilon^{vib}_{\parallel}$	$\epsilon^{vib}_{\perp}$	$\bar{\nu}_{calc}$	$\bar{\nu}_{exp}$	$\mathcal{I}_p$	$\epsilon^{vib}_{\parallel}$	$\epsilon^{vib}_{\perp}$	$\bar{\nu}_{calc}$	$\bar{\nu}_{exp}$	$\mathcal{I}_p$	ϵ^{vib}_{zz}	ϵ^{vib}_{yy}	ϵ^{vib}_{xx}
$i59$	52	×	×	×	59	44	-	-	-	52	44	268	42	-	48	44	-	-	-	-
$i58$	52	×	×	×	$i27$	11	×	×	×	$i22$	14	×	×	×	36	14	5760	3906	-	
$i31$	90	×	×	×	$i31$	90	×	×	×	91	90	5206	268	-	58	90	5454	-	689	-
$i24$	90	×	×	×	50	90	-	-	-	56	90	3034	-	210	71	90	5294	-	-	423
137	145	-	-	-	134	144	-	-	-	134	144	0.21	-	-	134	144	0.22	-	-	-
138	145	-	-	-	149	144	-	-	-	148	144	-	-	-	149	144	0.23	-	-	-
164	170	91	1.46	-	161	170	50	0.78	-	162	171	255	-	2.10	163	171	554	-	3.93	4.91
165	170	176	-	1.38	174	170	119	-	0.92	177	171	120	1.65	-	174	171	3.35	0.05	-	-
264	265	0.52	-	-	271	265	0.24	-	-	271	265	4.63	-	0.01	271	265	1.01	-	-	-
264	265	-	-	-	272	265	-	-	-	272	265	-	-	-	273	265	-	-	-	-
448	446	-	-	-	446	420	-	-	-	425	420	-	-	-	440	420	3.07	-	-	0.01
448	446	-	-	-	447	420	7.21	-	0.01	447	420	10.65	-	0.01	443	420	-	-	-	-
458	450	-	-	-	459	450	-	-	-	460	450	-	-	-	460	450	0.06	-	-	-
458	450	-	-	-	461	450	-	-	-	461	450	-	-	-	461	450	-	-	-	-
480	474	-	-	-	460	474	-	-	-	460	517	0.03	-	-	490	517	0.90	-	-	-
480	474	-	-	-	487	474	-	-	-	511	517	-	-	-	501	517	0.45	-	-	-
546	546	773	1.11	-	543	546	1518	-	1.09	544	546	1489	-	1.08	545	546	766	-	1.09	
546	546	1529	-	1.10	547	546	750	1.08	-	550	546	808	1.14	-	547	546	757	1.08	1.09	1.10
867	∼800	-	-	-	861	∼800	-	-	-	862	∼800	-	-	-	865	∼800	0.03	-	-	-
ϵ^{vib}			2.57	2.48				1.86	2.02				312.8	213.2				3907	695.1	429.2
ϵ^{el}			4.88	4.88				4.88	4.88				4.85	4.88				4.88	4.87	4.85

$I4cm$ and $Ima2$ ones. The vibrational contribution to the piezoelectricity is connected to the vibrational contribution to the dielectric tensor which can be computed analytically through Eq. (1). Phonon frequencies (expressed in wave numbers $\bar{\nu} = \nu/c$, with c speed of light), infrared intensities $\mathcal{I}_p$, and vibrational contributions to the dielectric tensor ϵ^{vib} are reported in Table III for the four structures considered, as obtained with the PBE0 hybrid functional. Experimental vibration frequencies are also reported.

For the cubic $Pm\bar{3}m$ phase, accurate measurements of the phonon frequencies are available[84,85] both for Γ-point and R-point phonons, which correspond to the BZ center frequencies of the pseudocubic structure reported in Table III. It is seen that, when vibration frequencies greater than 100 cm^{-1} are considered, the overall agreement between the computed and observed values is definitely satisfactory with an average discrepancy of 3 cm^{-1} and a maximum error of 8 cm^{-1}. The agreement is necessarily less satisfactory as regards low-frequency soft modes. The first mode in the list, with a calculated imaginary frequency of $i59$ cm^{-1}, is the R-point mode corresponding to the octahedra rotation. At room temperature this frequency is small and positive (see the experimental value) and it decreases by lowering the temperature until reaching zero at $T_a = 105$ K (Ref. 17): the computed values are "projected" at 0 K and then imaginary. The second and third imaginary frequencies correspond to the ferroelectric instability due to the Ti atoms' displacement. The corresponding soft modes are expected to be rather anharmonic and thus difficult to be properly described at the harmonic level. The vibrational contributions to the dielectric tensor are small (2.57 and 2.48 for the parallel and perpendicular components, respectively), compared to the experimental average value of 310 at room temperature[87] because the second and third modes' contributions (which would be significant due to their strong IR activity) have to be neglected due to their imaginary computed frequencies.

When passing from the cubic to the AFD tetragonal $I4/mcm$ phase, the agreement between the computed and measured phonon frequencies are slightly ameliorated; high-frequency modes remain almost unchanged while the first mode in the list (the TiO_6 rotation) that drives the transition at $T = 105$ K correctly becomes positive, 59 cm^{-1}, and comparable to the experimental value of 44 cm^{-1}. The two soft modes connected to the ferroelectric instability still show imaginary frequencies thus providing a small value for ϵ^{vib}, the same as for the cubic phase.

As concerns the ferroelectric phase, recent Raman measurements on $SrTi^{18}O_3$ have revealed peaks at 11, 17, and 17.5 cm^{-1} that correspond to a large set of very soft phonon modes which significantly affect many properties of the system.[34] While the second mode in Table III is still imaginary in the tetragonal $I4cm$ structure, it correctly becomes small and positive, 36 cm^{-1}, in the orthorhombic $Ima2$ one. As suggested by recent neutron scattering experiments and

TABLE IV. Elastic and compliance constants of the four structures considered of $SrTiO_3$. Electronic "clamped-ion" and total "relaxed," with nuclear contribution, constants are reported. The computed bulk modulus B is also reported. Calculations performed at the PBE0 level.

	Elastic Tensor $\mathbb{C}$ (GPa)									Compliance Tensor $\mathbb{S}$ (TPa^{-1})									
	C_{11}	C_{12}	C_{13}	C_{22}	C_{23}	C_{33}	C_{44}	C_{55}	C_{66}	S_{11}	S_{12}	S_{13}	S_{22}	S_{23}	S_{33}	S_{44}	S_{55}	S_{66}	B (GPa)
$Pm\bar{3}m$																			
Relaxed	370	114	114	370	114	370	133	133	133	3.16	−0.75	−0.75	3.16	−0.75	3.16	7.50	7.50	7.50	199
Clamped	370	114	114	370	114	370	133	133	133	3.16	−0.75	−0.75	3.16	−0.75	3.16	7.50	7.50	7.50	199
$I4/mcm$																			
Relaxed	371	109	116	371	116	366	132	132	125	3.13	−0.68	−0.78	3.13	−0.78	3.22	7.58	7.58	8.00	199
Clamped	371	109	116	371	116	366	132	132	125	3.13	−0.68	−0.78	3.13	−0.78	3.22	7.58	7.58	8.00	199
$I4cm$																			
Relaxed	371	108	112	371	112	282	121	121	124	3.19	−0.63	−1.01	3.19	−1.01	4.34	8.24	8.24	8.07	185
Clamped	371	109	116	371	116	365	130	130	125	3.13	−0.68	−0.78	3.13	−0.78	3.22	7.63	7.63	7.99	199
$Ima2$																			
Relaxed	298	60	115	330	117	364	131	120	89	3.84	−0.30	−1.12	3.43	−1.01	3.42	7.63	8.34	11.27	171
Clamped	370	110	116	371	116	367	131	131	126	3.15	−0.69	−0.77	3.14	−0.77	3.21	7.63	7.63	7.95	199

theoretical simulations, our phonon calculations also support the orthorhombic symmetry of the low-temperature ferroelectric phase of $SrTiO_3$ (Refs. 39,40). Both ferroelectric phases show a large IR activity and, consequently, a large vibration contribution to the dielectric tensor, particularly due to the two ferroelectric soft phonon modes (when positive). However, even for the orthorhombic phase, where all frequencies are positive, the value of ϵ^{vib} (3907 for the zz component) is still very small if compared to experimental values: about 10^4 for both the parallel and perpendicular components of $SrTiO_3$ in the low-temperature regime.[11,12] This underestimation is quite expected from the analysis of Eq. (1) where the vibration contribution to ϵ is clearly shown to be inversely proportional to ν_p^2; the largest contribution for the low-temperature phases comes from ferroelectric soft modes with experimental frequencies of 11 and 17 cm^{-1}. In our calculations such phonon frequencies are either imaginary or, in the orthorhombic phase, positive but not small enough.

C. Piezoelectricity

Direct and converse piezoelectricity measure the variation of polarization under a finite strain and the strain induced by an applied electric field, respectively. The two third-rank tensors associated with these properties, **e** and **d**, are connected to each other via the elastic $\mathbb{C}$ and compliance $\mathbb{S}$ tensors, according to relations (6). For this reason we start by analyzing such quantities.

In Table IV, we report the elastic and compliance constants of $SrTiO_3$ for the four structures here considered as computed with the PBE0 hybrid functional. The electronic "clamped-ion" contribution is separated from the total "relaxed" constants which include nuclear terms. The computed bulk modulus B is also reported. At first glance, it can be noticed that the "clamped-ion" contribution is essentially the same for every structure, with a bulk modulus always about 199 GPa. While the nuclear relaxation contribution is almost negligible for the cubic $Pm\bar{3}m$ and AFD tetragonal $I4/mcm$ phases, it becomes significant for the two ferroelectric phases where the bulk modulus decreases from 199 to 185 and 171 GPa for the tetragonal $I4cm$ and the orthorhombic $Ima2$ phases, respectively. The orthorhombic phase thus provides a larger elastic softening, again in better agreement with experimental observations.[10] Let us enter into more detail to interpret such an elastic softening: in the tetragonal phase, the softened constant is $C_{33} \equiv C_{zzzz}$ that passes from 365 to 282 GPa whereas in the orthorhombic phase $C_{11} \equiv C_{xxxx}$ from 370 to 298 GPa and $C_{22} \equiv C_{yyyy}$ from 371 to 330 GPa. This is due to the fact that while in the tetragonal structure Ti atoms are symmetry-constrained to move along the z direction, in the orthorhombic structure they can move in the xy plane, much more along x than along y. The same, even if inverse, reasoning holds true for the compliance constants.

In Table V, we report direct and converse piezoelectric constants of the two ferroelectric structures considered of $SrTiO_3$. As for elastic and compliance tensors, electronic "clamped-ion" and total "relaxed," with nuclear contribution, constants are reported. From an inspection of that table, a large effect of nuclear relaxation can easily be inferred. Direct piezoelectric constants are as large as 8.82 and 9.28 C/m^2 for the tetragonal and orthorhombic phases, respectively. Such a piezoelectric response is two orders of magnitude higher than that of α quartz, a standard piezoelectric material, whose largest constant e_{11} is 0.15 C/m^2 at room temperature and 0.07 C/m^2 down to 5 K (Ref. 88).

Let us consider, first, the tetragonal phase. A relatively small constant $e_{31} \equiv e_{zxx} = 0.20$ C/m^2 measures the polarization induced along z by a strain η_{xx}; nuclear relaxation doubles its value. The largest constant is $e_{33} \equiv e_{zzz}$ which passes from -0.13 to 8.82 C/m^2 after relaxation. This constant gives the variation of polarization along z when the crystal is strained along the same direction; the effect of nuclear relaxation is very large in this case (there is even a change of sign) because it directly involves the motion of Ti atoms along z (the ferroelectric soft phonon modes described in Sec. III B). When the crystal is deformed in the yz plane, a polarization appears along y that results in the $e_{24} \equiv e_{yyz} = 4.86$ C/m^2 constant which is also quite affected by nuclear relaxation. As anticipated in the Introduction, one of the few piezoelectric quantities already reported in the literature so far is $e_{33} - e_{31} \sim$

TABLE V. Direct and converse piezoelectric constants of the two ferroelectric structures considered of $SrTiO_3$. Electronic "clamped-ion" and total "relaxed," with nuclear contribution, constants are reported. Calculations performed at the PBE0 level.

	Direct Piezoelectricity **e** (C/m^2)								Converse Piezoelectricity **d** (pm/V)							
	e_{11}	e_{31}	e_{12}	e_{13}	e_{33}	e_{24}	e_{35}	e_{26}	d_{11}	d_{31}	d_{12}	d_{13}	d_{33}	d_{24}	d_{35}	d_{26}
$I4cm$																
Relaxed		0.20			8.82	4.86				−8.41			37.90	40.06		
Clamped		0.08			−0.13	0.05				0.29			−0.55	0.37		
$Ima2$																
Relaxed	9.28		6.70	0.20			4.61	6.04	33.51		20.08	−16.70			38.49	68.10
Clamped	0.02		−0.06	0.06			0.04	−0.09	0.04		−0.26	0.24			0.31	−0.69

6 C/m^2, to be compared with our value of 8.62 C/m^2 (Ref. 5). Converse piezoelectric constants are the result of a coupling between direct piezoelectric and compliance constants. In particular, the high relaxed value of d_{33} of 37.90 pm/V with respect to the purely electronic value of −0.55 pm/V is equally due, on the one hand, to the relaxation effect on e_{33} and, on the other hand, to the softening of the C_{33} elastic constant upon relaxation. The high value of d_{24} of 40.06 pm/V is dominated by e_{24} and less affected by the small softening of C_{44}.

In the orthorhombic $Ima2$ structure, Ti atoms can be displaced in the xy plane and not along the z direction; as a consequence, a larger number of high piezoelectric constants appears. The only relatively small constant $e_{13} = 0.20$ C/m^2 measures the variation of polarization along x when the crystal is strained along z and is the analog of $e_{31} = 0.20$ C/m^2 for the tetragonal structure. The largest constant is $e_{11} \equiv e_{xxx} = 9.28$ C/m^2 because Ti atoms can mainly be displaced along x. The two constants e_{12} and e_{26}, which measure the polarization induced along x and y by strains along y and in the xy plane, respectively, have similar values of 6.70 and 6.04 C/m^2. As regards the converse piezoelectricity, a very large constant $d_{24} \equiv d_{yyz} = 68.10$ pm/V is found which describes the strain η_{yz} induced in the structure by an external electric field applied along y. The effect of nuclear relaxation on this constant is very large (from −0.69 to 68.10 pm/V) and it is due to e_{24} and to the peculiar softening of the C_{66} elastic constant, from 126 to 89 GPa (see Table IV).

In conclusion, when a deformation is applied which involves a direction along which Ti atoms can be displaced, a large piezoelectric response is expected to arise in $SrTiO_3$ at low temperatures. When the corresponding ferroelectric phonon modes become very soft (as experimentally happens at very low temperatures), a giant piezoelectric response is measured.[3]

IV. CONCLUSION

A full characterization of the piezoelectricity of $SrTiO_3$ at low temperatures is performed by means of accurate *ab initio* simulations using the global hybrid functional PBE0. Four structures (the cubic $Pm\bar{3}m$, the antiferrodistortive tetragonal $I4/mcm$, a ferroelectric tetragonal $I4cm$, and a ferroelectric orthorhombic $Ima2$) are considered and their structural, vibrational, elastic, and piezoelectric properties computed and discussed.

Complete direct and converse piezoelectric tensors of the two ferroelectric structures are computed and their main features discussed. Electronic "clamped-ion" contributions are separated from fully nuclear relaxed data. The anomalously large zero-point motion of Ti atoms, connected to the ferroelectric instability, is found to largely affect the piezoelectric response of $SrTiO_3$. A much richer piezoelectric response is predicted to occur if the symmetry of the ferroelectric system is orthorhombic (as was recently theoretically suggested), rather that tetragonal. A complete experimental characterization of the piezoelectric tensor of $SrTiO_3$ is then expected to shed some light on the structural features of the still unknown symmetry of the ferroelectric low-temperature phase.

ACKNOWLEDGMENTS

The authors are grateful to Ahmed Redha Benrekia for helping with some preliminary calculations and to Roberto Dovesi for fruitful discussions.

*alessandro.erba@unito.it

[1] P. Panda, J. Mater. Sci. **44**, 5049 (2009).
[2] S. Zhang, R. Xia, L. Lebrun, D. Anderson, and T. R. Shrout, Mater. Lett. **59**, 3471 (2005).
[3] D. E. Grupp and A. M. Goldman, Science **276**, 392 (1997).
[4] T. Furuta and K. Miura, Solid State Comm. **150**, 2350 (2010).
[5] I. I. Naumov and H. Fu, Phys. Rev. B **72**, 012304 (2005).
[6] C. E. Ekuma, M. Jarrell, J. Moreno, and D. Bagayoko, AIP Advances **2**, 012189 (2012).
[7] H. P. R. Frederikse, W. R. Hosler, and W. R. Thurber, Phys. Rev. **143**, 648 (1966).
[8] W. Zhong, R. D. King-Smith, and D. Vanderbilt, Phys. Rev. Lett. **72**, 3618 (1994).
[9] W. Jauch and A. Palmer, Phys. Rev. B **60**, 2961 (1999).
[10] A. V. Kityk, W. Schranz, P. Sondergeld, D. Havlik, E. K. H. Salje, and J. F. Scott, Phys. Rev. B **61**, 946 (2000).
[11] T. Sakudo and H. Unoki, Phys. Rev. Lett. **26**, 851 (1971).
[12] K. A. Müller and H. Burkard, Phys. Rev. B **19**, 3593 (1979).

[13]N. Reyren, S. Thiel, A. D. Caviglia, L. F. Kourkoutis, G. Hammerl, C. Richter, C. W. Schneider, T. Kopp, A.-S. Retschi, D. Jaccard, M. Gabay, D. A. Muller, J.-M. Triscone, and J. Mannhart, Science **317**, 1196 (2007).
[14]A. Binder and K. Knorr, Phys. Rev. B **63**, 094106 (2001).
[15]H. Unoki and T. Sakudo, J. Phys. Soc. Jpn **23**, 546 (1967).
[16]A. Heidemann and H. Wettengel, Zeitschrift für Physik **258**, 429 (1973).
[17]A. Bussmann-Holder, H. Büttner, and A. R. Bishop, Phys. Rev. Lett. **99**, 167603 (2007).
[18]C. LaSota, C. Z. Wang, R. Yu, and H. Krakauer, Ferroelectrics **194**, 109 (1997).
[19]A. K. Tagantsev, E. Courtens, and L. Arzel, Phys. Rev. B **64**, 224107 (2001).
[20]R. A. Evarestov, E. Blokhin, D. Gryaznov, E. A. Kotomin, and J. Maier, Phys. Rev. B **83**, 134108 (2011).
[21]F. El-Mellouhi, E. N. Brothers, M. J. Lucero, and G. E. Scuseria, Phys. Rev. B **84**, 115122 (2011).
[22]N. Sai and D. Vanderbilt, Phys. Rev. B **62**, 13942 (2000).
[23]E. K. H. Salje, M. C. Gallardo, J. Jiménez, F. J. Romero, and J. del Cerro, J. Phys.: Condens. Matter **10**, 5535 (1998).
[24]W. Zhong and D. Vanderbilt, Phys. Rev. B **53**, 5047 (1996).
[25]K. A. Müller, W. Berlinger, and E. Tosatti, Z. Physik B Condensed Matter **84**, 277 (1991).
[26]P. A. Fleury and J. M. Worlock, Phys. Rev. **174**, 613 (1968).
[27]A. Devonshire, Adv. Phys. **3**, 85 (1954).
[28]H. Uwe and T. Sakudo, Phys. Rev. B **13**, 271 (1976).
[29]J. H. Haeni, P. Irvin, W. Chang, R. Uecker, P. Reiche, Y. L. Li, S. Choudhury, W. Tian, M. E. Hawley, B. Craigo, A. K. Tagantsev, X. Q. Pan, S. K. Streiffer, L. Q. Chen, S. W. Kirchoefer, J. Levy, and D. G. Schlom, Nature (London) **430**, 758 (2004).
[30]J. G. Bednorz and K. A. Müller, Phys. Rev. Lett. **52**, 2289 (1984).
[31]A. Chen, Z. Yu, J. Scott, A. Loidl, R. Guo, A. Bhalla, and L. Cross, J. Phys. Chem. Solids **61**, 191 (2000).
[32]M. Itoh, R. Wang, Y. Inaguma, T. Yamaguchi, Y.-J. Shan, and T. Nakamura, Phys. Rev. Lett. **82**, 3540 (1999).
[33]H. Taniguchi, M. Itoh, and T. Yagi, Phys. Rev. Lett. **99**, 017602 (2007).
[34]T. Shigenari, K. Abe, T. Takemoto, O. Sanaka, T. Akaike, Y. Sakai, R. Wang, and M. Itoh, Phys. Rev. B **74**, 174121 (2006).
[35]M. Kasahara, H. Hasebe, R. Wang, M. Itoh, and Y. Yagi, J. Phys. Soc. Jpn. **70**, 648 (2001).
[36]H. Hasebe, Y. Tsujimi, R. Wang, M. Itoh, and T. Yagi, Ferroelectrics **272**, 39 (2002).
[37]M. Yamaguchi, T. Yagi, Y. Tsujimi, H. Hasebe, R. Wang, and M. Itoh, Phys. Rev. B **65**, 172102 (2002).
[38]K. Yamanaka, R. Wang, M. Itoh, and K. Iio, J. Phys. Soc. Jpn. **70**, 3213 (2001).
[39]Y. Noda, K. Mochizuki, H. Kimura, M. Itoh, T. Kyomen, and R. Wang, J. Korean Phys. Soc. **46**, 69 (2005).
[40]M. Bartkowiak, G. J. Kearley, M. Yethiraj, and A. M. Mulders, Phys. Rev. B **83**, 064102 (2011).
[41]J. P. Perdew, K. Burke, and M. Ernzerhof, Phys. Rev. Lett. **77**, 3865 (1996).
[42]C. Adamo and V. Barone, J. Chem. Phys. **110**, 6158 (1999).
[43]R. Dovesi, V. R. Saunders, C. Roetti, R. Orlando, C. M. Zicovich-Wilson, F. Pascale, K. Doll, N. M. Harrison, B. Civalleri, I. J. Bush, Ph. D'Arco, and M. Llunell, CRYSTAL09 *User's Manual*, Università di Torino, Torino (2010), http://www.crystal.unito.it.
[44]R. Dovesi, R. Orlando, B. Civalleri, C. Roetti, V. R. Saunders, and C. M. Zicovich-Wilson, Z. Kristallogr. **220**, 571 (2005).
[45]The basis set used in this work can be found at http://www.crystal.unito.it/Basis_Sets/Ptable.html.
[46]J. P. Hay and W. R. Wadt, J. Chem. Phys. **82**, 270 (1984).
[47]F. Pascale, C. M. Zicovich-Wilson, R. Orlando, C. Roetti, P. Ugliengo, and R. Dovesi, J. Phys. Chem. B **109**, 6146 (2005).
[48]M. Prencipe, F. Pascale, C. Zicovich-Wilson, V. Saunders, R. Orlando, and R. Dovesi, Phys. Chem. Min. **31**, 559 (2004).
[49]S. Tosoni, F. Pascale, P. Ugliengo, R. Orlando, V. R. Saunders, and R. Dovesi, Mol. Phys. **103**, 2549 (2005).
[50]K. Doll, Comput. Phys. Commun. **137**, 74 (2001).
[51]K. Doll, V. R. Saunders, and N. M. Harrison, Int. J. Quantum Chem. **82**, 1 (2001).
[52]B. Civalleri, P. D'Arco, R. Orlando, V. R. Saunders, and R. Dovesi, Chem. Phys. Lett. **348**, 131 (2001).
[53]C. G. Broyden, J. Inst. Math. Appl. **6**, 76 (1970).
[54]R. Fletcher, Comput. J **13**, 317 (1970).
[55]D. Goldfarb, Math. Comput. **24**, 23 (1970).
[56]D. F. Shanno, Math. Comput. **24**, 647 (1970).
[57]C. M. Zicovich-Wilson, F. Pascale, C. Roetti, V. R. Saunders, R. Orlando, and R. Dovesi, J. Comp. Chem. **25**, 1873 (2004).
[58]A. Erba, M. Ferrabone, R. Orlando, and R. Dovesi, J. Comput. Chem. **34**, 346 (2013).
[59]C. Carteret, M. De La Pierre, M. Dossot, F. Pascale, A. Erba, and R. Dovesi, J. Chem. Phys. **138**, 014201 (2013).
[60]A. Erba, S. Casassa, R. Dovesi, L. Maschio, and C. Pisani, J. Chem. Phys. **130**, 074505 (2009).
[61]G. J. B. Hurst, M. Dupuis, and E. Clementi, J. Chem. Phys. **89**, 385 (1988).
[62]B. Kirtman, F. L. Gu, and D. M. Bishop, J. Chem. Phys. **113**, 1294 (2000).
[63]M. Ferrero, M. Rérat, R. Orlando, and R. Dovesi, J. Comp. Chem. **29**, 1450 (2008).
[64]M. Ferrero, M. Rérat, R. Orlando, and R. Dovesi, J. Chem. Phys. **128**, 014110 (2008).
[65]M. Ferrero, M. Rérat, B. Kirtman, and R. Dovesi, J. Chem. Phys. **129**, 244110 (2008).
[66]A. Erba, M. Ferrabone, J. Baima, R. Orlando, M. Rérat, and R. Dovesi, J. Chem. Phys. **138**, 054906 (2013).
[67]V. Lacivita, A. Erba, Y. Noël, R. Orlando, P. D'Arco, and R. Dovesi, J. Chem. Phys. **138**, 214706 (2013).
[68]J. Baima, A. Erba, M. Rérat, R. Orlando, and R. Dovesi, J. Phys. Chem. C **117**, 12864 (2013).
[69]X. Gonze and C. Lee, Phys. Rev. B **55**, 10355 (1997).
[70]R. Resta, Rev. Mod. Phys. **66**, 899 (1994).
[71]R. D. King-Smith and D. Vanderbilt, Phys. Rev. B **49**, 5828 (1994).
[72]J. F. Nye, *Physical Properties of Crystals* (Oxford University Press, Oxford, 1957).
[73]Y. Noël, C. M. Zicovich-Wilson, B. Civalleri, P. D'Arco, and R. Dovesi, Phys. Rev. B **65**, 014111 (2001).
[74]R. D. King-Smith and D. Vanderbilt, Phys. Rev. B **47**, 1651 (1993).
[75]D. Vanderbilt, J. Phys. Chem. Solids **61**, 147 (2000).
[76]W. F. Perger, J. Criswell, B. Civalleri, and R. Dovesi, Comput. Phys. Commun. **180**, 1753 (2009).
[77]G. Saghi-Szabo, R. E. Cohen, and H. Krakauer, Phys. Rev. Lett. **80**, 4321 (1998).
[78]A. Dal Corso, M. Posternak, R. Resta, and A. Baldereschi, Phys. Rev. B **50**, 10715 (1994).

[79]P. Canepa, R. Hanson, P. Ugliengo, and M. Alfredsson, J. Appl. Cryst. **44**, 225 (2011).
[80]J. Heyd, G. E. Scuseria, and M. Ernzerhof, J. Chem. Phys. **124**, 219906 (2006).
[81]Y. Abramov, V. Tsirelson, V. Zavodnik, S. Ivanov, and I. Brown, Acta Cryst. B **51**, 942 (1995).
[82]K. Van Benthem, C. Elsasser, and R. French, J. Appl. Phys. **90**, 6156 (2001).
[83]Y. Yamada and Y. Kanemitsu, Phys. Rev. B **82**, 121103 (2010).
[84]W. G. Stirling, J. Phys. C **5**, 2711 (1972).
[85]J. L. Servoin, Y. Luspin, and F. Gervais, Phys. Rev. B **22**, 5501 (1980).
[86]P. Fleury, J. Scott, and J. Worlock, Phys. Rev. Lett. **21**, 16 (1968).
[87]W. G. Spitzer, C. Miller, D. A. Kleinman, and L. E. Howarth, Phys. Rev. **126**, 1710 (1962).
[88]R. Tarumi, K. Nakamura, H. Ogi, and M. Hirao, J. Appl. Phys. **102**, 113508 (2007).